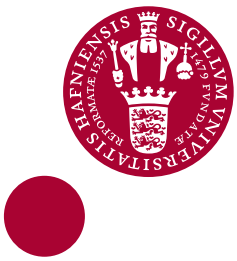

Microheterogeneities of redox states of perfused and intact organs.

Quistorff, Bjørn; Chance, Britton; Barlow, Clyde; Haselgrove, John; Nakase, Yuzo; Matschinsky, Franz; Mayevsky, Avraham

Published in:
Academic Press. Inc.

Publication date:
1978

Document version
Publisher's PDF, also known as Version of record

ACADEMIC PRESS RAPID MANUSCRIPT REPRODUCTION

A Virginia Lazenby O'Hara Biochemistry Symposium
held January 16–17, 1978
Dallas, Texas

Microenvironments and Metabolic Compartmentation

Edited by

Paul A. Srere
Ronald W. Estabrook

Veterans Administration Hospital
and
Department of Biochemistry
Southwestern Medical School
University of Texas Health Science Center
Dallas, Texas

ACADEMIC PRESS NEW YORK SAN FRANCISCO LONDON 1978
A Subsidiary of Harcourt Brace Jovanovich, Publishers

MICROHETEROGENEITIES OF REDOX STATES OF PERFUSED AND INTACT ORGANS

Britton Chance
Clyde Barlow
John Haselgrove
Yuzo Nakase
Bjørn Quistorff
Franz Matschinsky
Avraham Mayevsky

Johnson Research Foundation
University of Pennsylvania
Philadelphia, Pennsylvania

Microheterogeneity or metabolic activity is an essential property of some tissues in the normal state and of many in pathological states. Rapid methods for nondestructive, non-invasive evaluation of metabolic heterogeneity due to spatio-temporal variations of metabolic activity can most readily be evaluated by a two-dimensional flying spot scanner that reads out in real-time a histogram display of the distribution of redox states as measured by the fluorescence of mitochondrial flavoprotein or NADH. Another nondestructive technique is that of ^{31}P NMR which, while global in its signal averaging, discriminates the pH value of different tissue compartments. Three dimensional resolution of metabolic microheterogeneity can be obtained by redox scanning and sectioning of tissues in appropriate states of heterogeneity, for example, model infarcts of heart, metabolic states of liver, and local ischemias of brain. Sections scanned at distances of 100 microns can be assembled into three dimensional displays of tissue volumes in which homogeneous redox states are obtained. Microanalytical biochemistry using 50 ng samples gives results which control and amplify those of redox scanning.

I. INTRODUCTION

The classical approach of analytical biochemistry and indeed of surface fluorometry has been to average the metabolic states of all the cells in the particular tissue under

ISBN 0-12-660550-5

observation (1). Scanning micro-fluorometry of NADH fluorescence of the brain cortex (2) and more recently the development of 2- and 3-D redox scanning procedures for NADH and flavoprotein (Fp)(3), together with the deoxyglucose labelling techniques (4) clearly show the intrinsic complexity and heterogeneity of cell and tissue metabolism as suggested by other methods (5).

The apparently tried and true concept of homogenization of cells and tissues that made it possible to obtain large samples appropriate to the low sensitivities of the method apparently obscured the real distribution of metabolic states prior to homogenization. There are two types of heterogeneity that are readily demonstratable; temporal and spatial.

A. Temporal Heterogeneity

Metabolic oscillations (Figure 1) have been studied together with Estabrook (6) and Hess (7) in yeast cell suspensions and found to occur in heart (8) and in heart extracts by Frenkel (9). Here the amplitude of the oscillations is so large that ignoring the temporal heterogeneity would lead to "nonsense" assays in biochemical recording. In optical recording the assays can be timed to occur at the peaks or nodes of the oscillatory cycle (10) and thus be extremely useful.

B. Spatial Heterogeneity

The current discussion and the papers at this symposium emphasize inhomogeneities of distribution of enzymes in the liver lobule and the consequent differences of metabolism in different parts of the liver lobule (5,11).

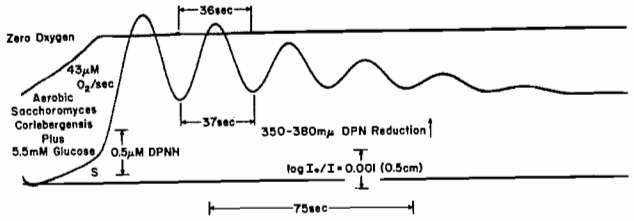

FIGURE 1. Temporal heterogeneities of metabolic control: NADH oscillations in anaerobic yeast cells (Saccharomyces carlsbergensis).

C. Spatio-temporal Heterogeneity

Spatio-temporal heterogeneities may occur in unstirred solutions as in Prigogine's "phase separations" (12), and in solid tissues as for example in the propagated disturbances such as spreading depression or epilepsy in the brian (13,14) (Figure 2). Preliminary spectroscopic observations of cytochrome a and oxymyoglobin indicated spatio-temporal heterogeneities of O_2 delivery to perfused heart (15).

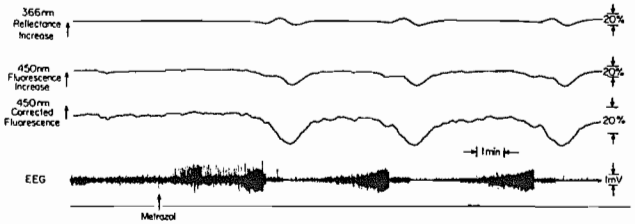

FIGURE 2. NADH oscillations due to spatio-temporal metabolic heterogeneity represented by periodic electrical and metabolic activity introduced by an intravenous metrazol injection in an anesthetized rat (Unpublished data of Mayevsky, A. and Chance, B.)

II. METHODOLOGICAL ASPECTS

A. Localized Indicators of Metabolic Activities

The identification of heterogeneities requires resolution of the metabolic state to intracellular dimensions and for this purpose mitochondria have proved themselves to be appropriate indicators of the metabolic intensity in tissue, affording a "consumer report" on metabolic activity and tissue oxygen delivery. The responses in various metabolic states are indicated by Figure 3A which indicates the correlation between metabolic state (16,17) and oxidation-reduction level of reduced pyridine nucleotide. Since oxygen delivery to tissue is intrinsically discrete and heterogeneous due to the nature of the capillary bed, changes in response to variations of the oxygen concentration (Figure 3B) are very useful. A quantitation of this response is indicated in Figure 3D, which shows how the pyridine nucleotide component (NADH) is a more sensitive indicator of tissue oxygen tension than is cytochrome c.

The most important aspect of the PN response is that it precisely follows the energy coupling response for mitochondria and thus serves as an indicator of both oxygen tension and energy coupling (18,19).

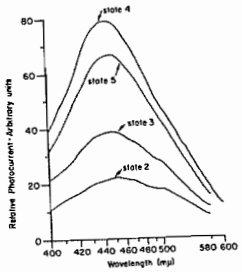

FIGURE 3A. Effect of metabolic state upon NADH redox level in rat liver mitochondria (18).

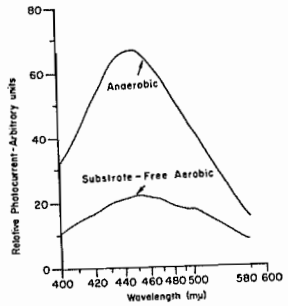

FIGURE 3B. Effect of oxygen upon NADH fluorescence in rat liver mitochondria (18).

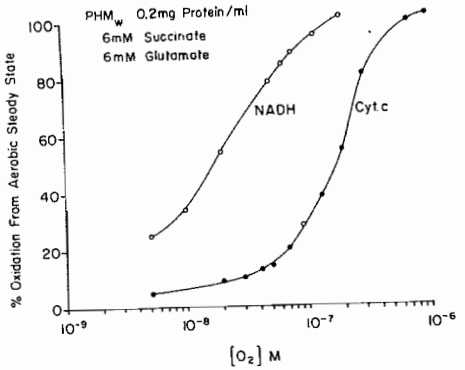

FIGURE 3C. A titration of NADH and cytochrome c with oxygen in isolated mitochondria (19).

B. The Flavoprotein Component of Mitochondria

The excitation-emission spectra for NADH and flavoprotein are compared in Fig. 4 which indicates that the oxidized state of flavoprotein will be observed exclusively in oxidized mitochondria whereas in reduced mitochondria, the pyridine nucleotide component is exclusively observed. Thus the ratio of the two signals gives a redox ratio largely independent of distribution and screening errors (20). These excitation-emission spectra were taken at low temperatures, although background pigments interfere more at the higher temperature.

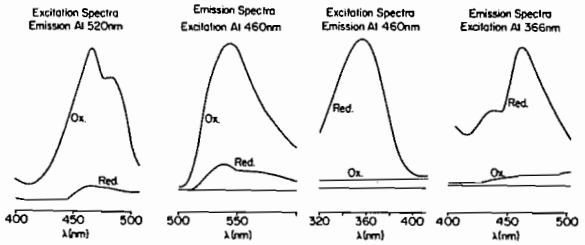

FIGURE 4. Low temperature excitation-emission spectra for PN (365 → 460 nm) and Fp (460 → 520 nm) for cardiac mitochondria (pigeon).

The localization of the highly fluorescent flavoprotein signal is within the mitochondrial space with the α-ketoglutarate and pyruvate dehydrogenases. The NADH signal at low temperature originates almost exclusively from the mitochondrial space while at room temperature in the perfused liver NADH signals may also be observed from the cytoplasm and from the NADPH pool.

C. Two-dimensional Ratio Recording

By time-sharing the excitation-emission wavelengths for Fp and PN it is possible to obtain signals from tissues whose ratio will represent the redox state of the material. The calibration procedure is described elsewhere (21). Such an instrument coupled to a lightguide of 20 to 80 microns in tip diameter can be used to scan a smoothed tissue section as indicated in the diagram of Figure 5.

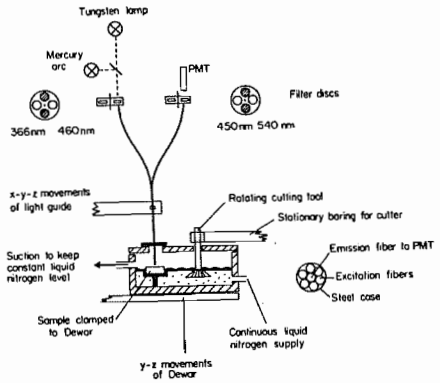

FIGURE 5. Illustrating the method of time-sharing Fp and PN signals, 2-D lightguide scanning of tissue section, and low temperature grinding of tissue surface for scans of consecutive sections.

The motion of the lightguide across the tissue is precisely controlled by a computer and Fp/PN fluorescence ratio recordings are acquired from over the surface of the tissue section. When one scan is finished the tissue may be ground in the rotating mill (22) and sections between 20 and 50 microns may be removed. The scan is then repeated so that a series of sections is accumulated, affording a series of 2-D presentations which can be displayed in 3-D.

III. RESULTS

A. Metabolic Heterogeneity in Cardiac Ishemia

The topical question of the nature and extent of the border zone in cardiac infarcts (23 - 25) is clarified by a series of sections of heart tissue containing a model coronary occlusion that are displayed in Figure 6. It seems that each one of the successive 100 μ tissue sections has borders that are quite sharp, as sharp as the 80 μ resolution of the scanner. In addition, the shape of the model infarct can be followed from the epicardium to the endocardium (see Figure 9).

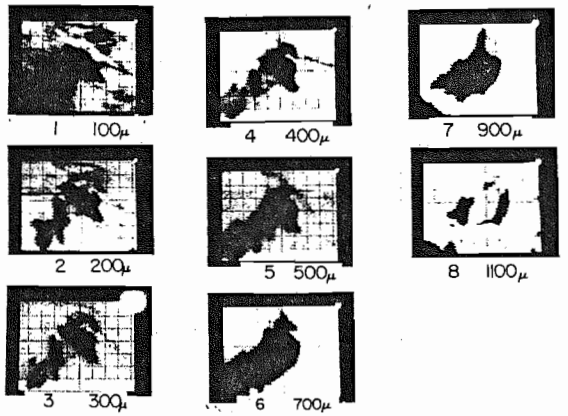

FIGURE 6. Consecutive 2-D scans of a model cardiac infarct from epi- to endocardium. The initial layer of the heart is scanned by the Fp/PN fluorometer at 80 μ resolution and the results are plotted as a 2-D redox picture with the reduced state black (low Fp/PN ratio) and the oxidized state white (high Fp/PN ratio). The initial scan represents a surface somewhat distorted by freeze-clamping, but later surfaces clearly outline the shape of the infarct proceeding from 100 μ below the epicardium to the endocardium (section 8).

B. The Steepness of the Border Zone in Model Infarcts

(a) Redox measurements

In order to compare three methods for evaluating the nature of the border zone, redox data are presented in Figures 7 and a combination of redox and analytical biochemical data in Figure 8. In Figure 7 a model coronary occlusion has been applied to a rabbit heart, the heart has been freeze-trapped and sectioned across the model infarct. Five identifying dots (actually drilled holes) appear as indices for the subsequent analysis. Figure 7A illustrates the use of NADH flash photography as applied to the freeze-trapped tissue; the bright areas represent reduced NAD and the dark areas oxidized NAD. The center mark of the indices is the reference point for the three subsequent displays (Figures 7B-D) illustrating the use of the lightguide scanner in evaluating the redox state of the ischemic and normoxic areas as was employed in the scan of Figure 6. Figure 7B shows the scan for NADH fluorescence. Contours of

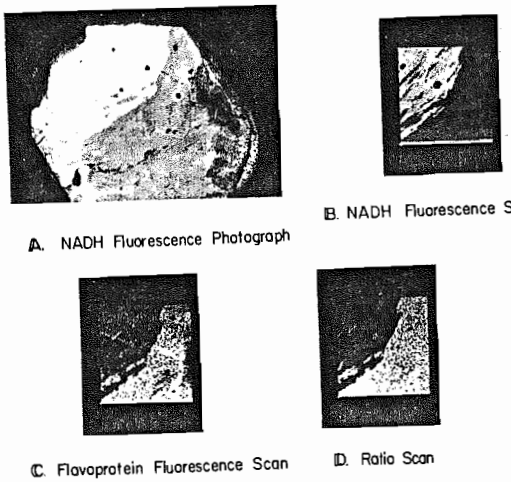

FIGURE 7. Comparison of redox scanning methods on a freeze-trapped section of rabbit heart with model coronary occlusion. A, NADH flash photography. B, Lightguide scan, NADH excitation and emission. C, Lightguide scan, flavoprotein excitation and emission. D, Lightguide Fp/PN ratio. Note that the central marker of the left figure appears in each one of the subsequent ones.

the border zones of Figures 7A and 7B are nearly identical testifying to the equality of performance of the two methods for 2-D NADH assay. Figure 7C is the scan of the ischemic and the normoxic areas with excitation and emission appropriate to flavoprotein and the figure is clearly complementary to Figure 7B. This illustrates how the ratio of these two quantities (Figure 7D) gives a redox state diagram less dependent upon variable distribution of mitochondria or an effect of screening pigments as indicated by the "smoothing" of the irregular signals introduced by the index signals in the heart.

Figure 8 displays quantitative analysis of the NADH scan of Figure 7B (circled dots) showing the rise of NADH fluorescence as one progresses from the dark aerobic portion to the index marker in the bright ischemic portion. The trace rises from 20-80% in a distance of 200 μ.

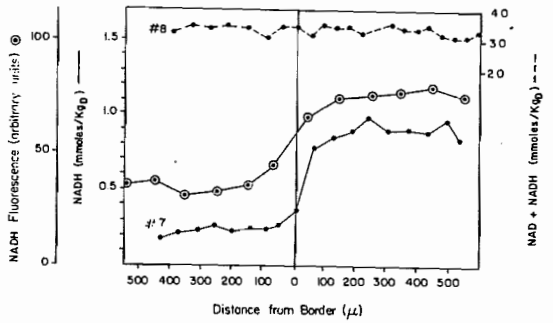

FIGURE 8. A comparison of the border zone delineated by redox scan of Figure 7B (Circle dot) and microanalytical biochemistry of NADH (solid trace) with total pyridine nucleotides (dashed trace). The microtome sections were 15 μ apart. The NADH assay (solid) was 105 μ below the surface of that represented by Figure 7. The top trace (dashes) was 120 μ below the surface.

(b) Microanalytical biochemistry

Microanalytical biochemistry can also be used to define the border between the two zones. Analyses of NADH (solid trace) is made along the same line across the border zone of the same specimen, but a section deeper below the surface; the particular section was 105 μ below the surface of Figure 7 and was 15 μ thick. The sample volume was 50 ng and and each point corresponds to a different sample. A quantitative assay in terms of millimoles per kilo dry weight (m moles/kg_D) is afforded. The two traces are very similar and both give the same contour for the border zone. In order to ensure that no pyridine nucleotides were lost from the ischemic portion of the heart under the conditions of the experiments, the top trace gives the total of NAD plus NADH which is maintained at 3 millimoles per kg dry weight.

These data clearly identify the border zone in rabbit heart to involve the transition from normal aerobic respiring tissue to ischemic anoxic tissue in a distance of 200 μ. It appears that adequate resolution is obtainable from both redox scanning and analytical biochemistry to precisely identify the position of the border zone between normoxic and anoxic ischemic areas in model cardiac infarcts.

These values may be compared to the distance of 8-15 mm obtained by Hearse, et al (24) who used a much larger sample volume in the dog heart. Presumably the use of more highly

resolved analytical techniques would give sharper border zones in model infarcts in the dog heart.

(c) Three dimensional redox display

The possibility of a three dimensional display of such data has been explored recently and an assembly of the sections of Figure 6 are displayed in Figure 9. Here sections corresponding to the border zone of the 8 scans of Figure 6 are displayed in the three dimensional series giving the general shape of the infarct proceeding from the endocardial side to the epicardial side. Each section in this figure is 100 μ thick, very nearly equal to the maximum depth from which fluorescent signals can be obtained from the frozen tissue. For this reason, no correction for material lying at a depth greater than 100 μ from the surface of the frozen heart is necessary.

One of the noteworthy features of the three dimensional display is that the ischemic area does not appear to increase in size as one proceeds from the epicardium to the endocardium. Thus, we have demonstrated the general principles of the redox scanning combined with the micro-analysis and its applicability to a variety of systems.

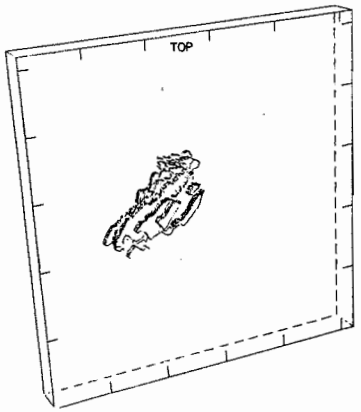

FIGURE 9. A 3-D assembly of sections 2-D of the infarct of Figure 6 from endo- to epicardium.

B. Kinetics of Changes in Two-dimensional Metabolic Heterogeneity

As convenient as the 3-D method is, the data are based upon one sample of tissue trapped at a moment of time and does not permit further following the metabolic events in that particular portion of the organ. For this reason we have considered a method that would read out in real time the metabolic heterogeneity from the surface of the organ in order to provide a maximally "interesting" metabolic state (presumably one in which there is maximal deviation from the average) for freeze-trapping analytical biochemistry and redox scanning (3,25,26). The principles of the scanner are indicated in Figure 10. Here, a source illuminates two vibrating mirrors which afford a faster scan over the sample of about 1 cm^2 in area. The fluorescent light is focused by a Fresnel lens, measured by a photomultiplier via a secondary filter. The analysis circuit provides a histogram of the intensity of the signal versus the number of signals having a given intensity level for 64 levels. 20,000 points may be gathered in one second to form an extremely precise histogram.

Using laser light appropriate to the excitation of reduced pyridine nucleotide (350/363 nm) or flavoprotein (457.9 nm) it is possible to generate histograms for both of these pigments as shown in Figure 11 for a perfused liver.

In this case the histograms for the normoxic state have been matched so that they are superimposed one upon the other for the condition of normal flow through the liver (30 ml/min). If the flow is diminished to 5 ml/min the pyridine nucleotide fluorescence increases while the flavoprotein fluorescence

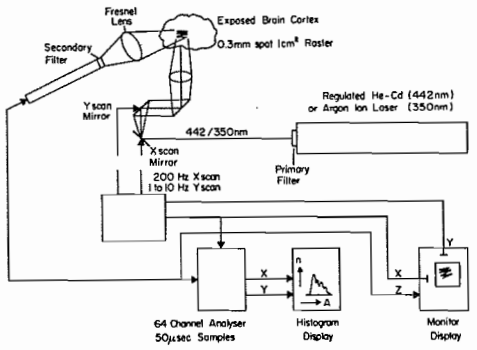

FIGURE 10. Block diagram of 2-D flying spot fluorometer with on-line histogram display.

decreases. The diagrams show how pyridine nucleotide and flavoprotein change in their respective opposite directions. Changes of heterogeneity are indicated also. In the anoxic state, the reduced pyridine nucleotide histogram becomes broader and the flavoprotein histogram becomes narrower.

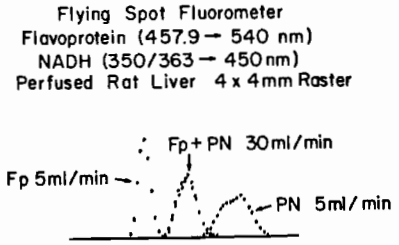

FIGURE 11. Illustrating the opposite response of Fp and PN histograms in a high-flow, low-flow hypoxia of a perfused rat liver.

C. Perfused Heart

The application of this technique to the heterogeneity of perfused heart is indicated in terms of flavin fluorescence in Figure 12. The normoxic histogram is distributed over most of the register as indicated in the left-hand diagram. This is characteristic of the "average" perfused heart where micro-heterogeneities in the redox pattern are due to small ischemic areas. In diagram B a major ischemic is imposed upon the heart by occlusion of a portion of the coronary artery resulting in intracellular anoxia in a portion of the tissue under observation. The histogram maintains its characteristics at 15, 30 and 60 sec. Thereafter, the ligature is released and the recovery pattern 5 min later is nearly identical to that prior to the coronary occlusion.

The difference of the two histograms is emphasized by the superimposed diagrams of Figure 12D. A cut-out and weighing of the differences between the two portions indicates that 20% of the area scanned is rendered anoxic by the model infarct. Those portions affected mostly by the model infarct are those having the highest fluorescence intensity and hence the most normoxic state. These histograms are recorded once every second but can be recorded in 0.1 sec. Thus, the mirror scan can be synchronized with the heart beat so that the histogram can be attributed to systole or diastole.

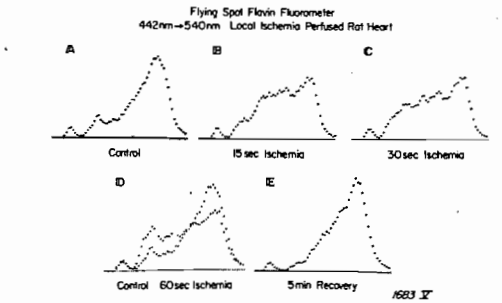

FIGURE 12. Changes of Fp histogram of a perfused rat heart following a model coronary occlusion.

D. Metabolic Heterogeneities in Brain Tissue

Scans of a portion of the left brain cortex of a gerbil (Fig. 13 - experiments in collaboration with A. Mayevsky) indicate in the top left-hand diagram the histogram in response to NADH fluorescence excitation in normoxia (left) and anoxia (30 sec).

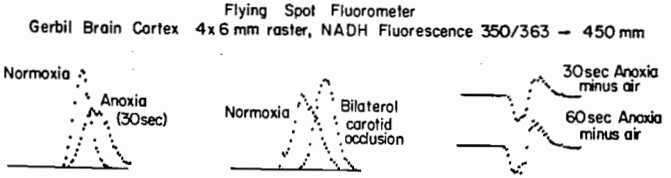

FIGURE 13. Comparison of NADH histograms of gerbil brain before and after bilateral carotid artery occlusion and systemic anoxia

The normoxic histogram which extends over 65% of the scale is replaced by the anoxic histogram which extends over 62% of the scale. The heterogeneity of NADH redox states in anoxia seems significantly greater than that of normoxia as indicated by the smaller height and greater breadth of the anoxic histogram. Since the blood flow to the gerbil brain is largely delivered by the carotid arteries, bilateral occlusion gives an almost complete anoxia as indicated in the right-hand diagram. However the heterogeneity of the ischemic tissue is less , the amplitude is larger and the base of the histogram subtends only 58% of the scale. Thus a quantitative difference between a systemic anoxia and low flow ischemia is indicated by the simple histogram technique.

E. Flavoprotein Fluorescence of Perfused and in situ Liver.

The application of the flying spot flavin fluorometer to the evaluation of heterogeneity of redox states in the perfused liver is indicated in Figure 14.

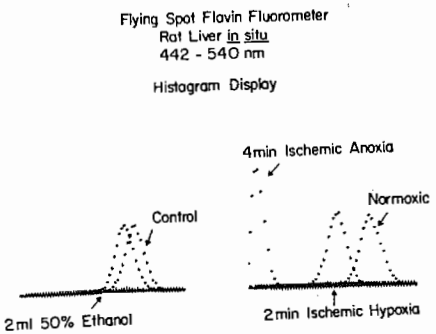

FIGURE 14. Histogram displays of metabolic changes of Fp in rat liver in situ.

On the right are three histograms indicating the progression from normoxia (extreme right), two minutes ischemia, and four min. ischemia (approximately 50% shift to the left). (The zero point of the histogram scale is set at 50% in this particular case to provide amplifications of the histograms). The remarkable feature here is the considerably greater homogeneity of the anoxic state of liver as measured by flavoprotein fluorescence. This might be expected, however, since in anoxia the flavoprotein of the α-ketoglutarate and pyruvate dehydrogenases has no other metabolic pathways to participate in.

On the left is indicated the response of the Fp redox state to injection of a high concentration of alcohol into the stomach. After 30 min. it is seen that the histogram shifts to the left indicating reduction. In this case, however, there is no change of heterogeneity of the metabolic states, apparently in this case those mitochondria metabolizing alcohol have the same heterogeneity characteristics as in the absence of alcohol.

These examples are afforded in order to give some idea of how a two-dimensional flying spot scanner can be used to select appropriate deviations of metabolic states by 2-D redox scanning and micro-analytical biochemistry.

F. ^{31}P Nuclear Magnetic Resonance

THe fourth approach to be described is that of ^{31}P nuclear magnetic resonance, Figure 15.

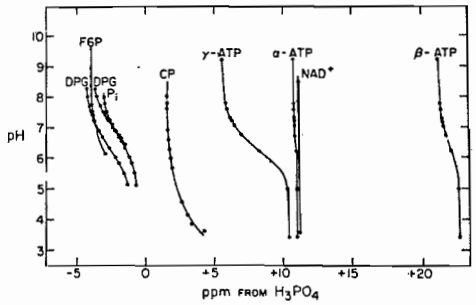

The pH-dependent chemical shift behavior of a variety of biological organic phosphates. Chemical shifts are reported relative to external 1.0 M phosphoric acid. *F6P*, fructose 6-phosphate; *DPG*, 2,3-diphosphoglycerate; *CP*, carbamyl phosphate.

FIGURE 15. Courtesy of Journal of Biological Chemistry (Ref. 27).

As shown, there is a pH dependence of several of the signals that are likely to be present in aerobic cells, particularly ATP and the sugar phosphates. Such signals have been obtained from skeletal muscle[28,29] and perfused heart.[30,31] The most prevalent signal of the anaerobic cell is inorganic phosphate and the chemical shift with decreasing pH is clearly shown by this diagram. The shift of the signal has been used to indicate intracellular pH.

In order to indicate the performance that is now obtainable from perfused organs, Figure 16 illustrates the ^{31}P nuclear magnetic resonance signals obtained from a perfused liver in the wide bore 360 megahertz (protons) NMR recently added to the Eastern Regional NMR Facility at the University of Pennsylvania.

Clearly shown in this diagram are resonances due to α, β, γ ATP and α ADP as well. The two peaks of phosphate are attributed to the pH 7.4 of the perfusate and somewhat less (~0.3 unit) for the intracellular P_i. The salient feature of the intracellular phosphate peak is its spread suggesting a heterogeneity of phosphate enviroments, most probably the cytosolic phosphate and the mitochondrial phosphate. While these signals are not well resolved under these conditions, further studies will lead to eventual resolution of the phosphate compartments of the metabolizing tissue.

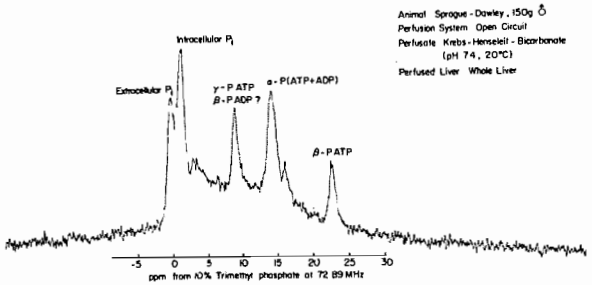

FIGURE 16. ^{31}P NMR spectrum of aerobic rat liver (perfused) (Experiments in collaboration with Dr. George MacDonald and Ms. M. Bond)

IV. DISCUSSION

The ability to cope with microheterogeneity of metabolic states of tissues and organs is in its infancy and the four techniques described here are at the beginning of their scientific application to the manifold problems presented to the biochemist in his new departure to metabolic heterogeneity. Recognizing the great usefulness of enzyme distribution, it has nevertheless been essential to consider the redox ratios of key couples of both glycolysis and respiration. In order to begin with the problem of metabolic heterogeneity it has been essential to develop "short cut" methods for evaluating the nature and extent of the heterogeneity before attempting more detailed procedures. For this reason we consider the on-line direct readout capability of the two dimensional flying spot fluorometer to be a key starting point in investigations of metabolic heterogeneity. The instrument is designed specifically to examine the time course of heterogeneities through a variety of metabolic transitions and therefore identify what we choose to term "maximal deviation metabolic states". A similar approach can be obtained through the use of ^{31}P NMR by observations of microheterogeneity of the phosphate resonance or possibly the ATP and sugar phosphate resonances. At the present time, the ^{31}P NMR method gives clear signals from extracellular and intracellular phosphate pools for the perfused liver, yet lacks the ability to split the intracellular compartment. The three dimensional problem of organ metabolism is one involving the acquisition of tremendous amounts of data either by redox scanning of successive sections of tissue or by laborious microanalytical biochemistry. The two methods are seen here to complement one another, the three dimensional redox scanning is a relatively rapid method of data acquisition, 10,000 analyses can be obtained in approximately 10min. Such redox scans identify the border zone between ischemic and anoxic

regions, for example, in model cardiac infarcts, and can be of value as well in any other perfused or in situ organs or tissues. Thus, preliminary observations with two dimensional redox scanning will identify tissue sections which fulfill the above mentioned criterion of "maximal deviation metabolic states" and thus indicate the portions of the tissue on which microanalytical biochemistry is appropriate. For example, in Figure 8, all the information on the transition from ischemic to normoxic tissues could have been obtained with microanalysis of the regions at 200 microns on either side of the border zone.

ACKNOWLEDGEMENTS

This work was supported in part by USPHS Grants HL-18708 and NS-10939. The help of Dr. George MacDonald is gratefully acknowledged.

REFERENCES

1. Bergmeyer, H.U. in *Methods of Enzymatic Analysis* (Bartley, W. ed.), Academic press, New York, 1963.
2. Stuart, B., and Chance, B., *Brain Res. 76*:473-479 (1974).
3. Quistorff, B. and Chance, B., in *Oxygen and Physiological Function* (Jöbsis, F.F., ed.) Professional Information Library Dallas, Texas, 1976. pp. 100-110.
4. Reivich, M., Sokoloff, L., Gunsberg, M.D., *Proc. Third Symp. on Cerebral and Coronary Vascular Disorders and Infarcts.* 1978. In press.
5. Matschinsky, F., *this volume.*
6. Chance, B., Estabrook, R.W., Ghosh, A., *Proc. Nat'l. Acad. Sci., USA 51*:1244 (1964).
7. Chance, B., Hess, B. and Betz, A., *Biochem. Biophys. Res. Comm. 16*:182 (1964).
8. Chance, B., Williamson, J.R., Jamieson, D., and Schoener, B. *Biochem. Zeit. 341*:357-377 (1965).
9. Frankel, R., *Biochem. Biophys. Res. Comm. 21*:497 (1965).
10. Betz, A., Chance, B., Schoener, B., Elsaesser, S., *J. Biol. Chem. 240*:3170-3181 (1965).
11. Rappaprot, A.M. in *The Liver, Vol. 1* (Roullier, ed.), Ch. Acad. Press, New York and London, 1963. p. 265.
12. Prigogine, I., in *Thermodynamics Theory of Structure, Stability and Fluctuations*, (Glansdorff, P. and Prigogine, I., eds.) Wiley, Interscience, New York, 1971.
13. Leao, A.A.P., *J. Neuro. Physiol.* 7:359-390 (1944).
14. Mayevsky, A., and Chance, B., *Brain Res. 98*:149-164, 1975.

15. Tamura, M., Oshino, N. and Chance, B., in *Oxygen Transport to tissue III* (Silver, I.A., Erecinska, M. and Bicher, H.I. eds.) Plenum Press, New York, 1979. pp. 85-101.
16. Chance, B., Schoener, B., and Schlinder, F. in *Oxygen in the Animal Organism* (Dickens, F. and Neil, E., eds.) Pergamon Press, Oxford, 1965. pp. 367-392.
17. Chance, B., and Williams, G.R., *J. Biol. Chem. 217*:409-427 (1955).
18. Chance, B. and Baltscheffsky, H., *J. Biol. Chem. 233*:736 (1958).
19. Sugano, S., Oshino, N. and Chance, B., *Biochim. Biophys. Acta 347*:340-358 (1974).
20. Chance, B., Lee, I.Y. and Oshino, N., *Fed. Proc. 35(3)*525 (1975). Abstr. 1757.
21. Chance, B., Takada, H., Nakase, Y., Itsak, F. *Fed. Proc. 38* 1978 (in press).
22. Ouistorff, B. and Chance, B. in *Oxygen Transport to Tissue III* (Silver, I.A., Erecinska, M. and Bicher, H.I., eds.) Panum Pub'l., New York. 1978.
23. Chance, B., *Suppl. to Cir. Res. 38-9* (Wildentahl, K., Morgan, H.E., Opie, L.H. and Srere, P.A., eds.) 1976. pp. I69-I71.
24. Hearse, D.J., Opie, L.H., Katzeff, I.E., Lubbe, W.F., van der Werff, T.J., Peisach, M., and Boulle, G., *Am. J., Cardiology 40*:716-726 (1977).
25. Barlow, C.H. and Chance, B., *Science 193*:909-910 (1976)
26. Chance, B., Barlow, C., Nakase, Y, Takeda, H., Mayevsky, A., Fischetti, R., Graham, N. and Sorge, J., *Am. J. Physiol.*, submitted March 1978.
27. Moon, B. and Richards, J.H., *J. Biol. Chem. 248*:7276-7278 (1973).
28. Dawson, J., Gadian, D.G. and Wilkie, B.R., *J. Physiol. 258* 823-833 (197).
29. Burt, C.P., Glonek, T. and Bárány, M., *Science 195*:145-149 (1977).
30. Gadian, D.G., Hoult, D.I., Radda, G.K., Seeley, P.J., Chance, B. and Barlow, C.H.B., *Proc. Nat'l. Acad. Sci, USA 73*:4446-4448 (1976).
31. Jacobus, W.E., Taylor, IV, G.J., Hollis, D.P., Nunnally, R. L., *Nature 265*:756-758 (1977).